ACS NANO

www.acsnano.org

ARTICLE

Ex-Solution Hybrids Functionalized on Oxide Nanofibers for Highly Active and Durable Catalytic Materials

Dong-Ha Kim,[†] Jun Kyu Kim,[†] DongHwan Oh, Seyeon Park, Yong Beom Kim, Jaehyun Ko, WooChul Jung,* and Il-Doo Kim*

Cite This: *ACS Nano* 2023, 17, 5842−5851

Read Online

ACCESS | Metrics & More | Article Recommendations | Supporting Information

ABSTRACT: **Ex-solution catalysts containing spontaneously formed metal nanoparticles socketed on the surface of reservoir oxides have recently been employed in various research fields including catalysis and sensing, due to the process efficiency and outstanding chemical/thermal stability. However, since the ex-solution process accompanies harsh reduction heat treatment, during which many oxides undergo phase decomposition, it restricts material selection and further advancement. Herein, we propose an elaborate design principle to uniformly functionalize ex-solution catalysts at porous oxide frameworks via an electrospinning process. As a case study, we selected the ex-solved $La_{0.6}Ca_{0.4}Fe_{0.95}Co_{0.05-x}Ni_xO_{3-\delta}$ (x = 0, 0.025 and 0.05) and SnO_2 nanofibers as ex-solution hybrids and main frameworks, respectively. We confirmed superior dimethyl sulfide (C_2H_6S) gas sensing characteristics with excellent long-cycling stability. In particular, the high catalytic activities of ex-solved CoNiFe ternary nanoparticles, strongly socketed on reservoir oxide, accelerate the spillover process of O_2 to dramatically enhance the response toward sulfuric analytes with exceptional tolerance. Altogether, our contribution represents an important stepping-stone to a rational design of ex-solved particle-reservoir oxide hybrids functionalized on porous oxide scaffolds for a variety of applications.**

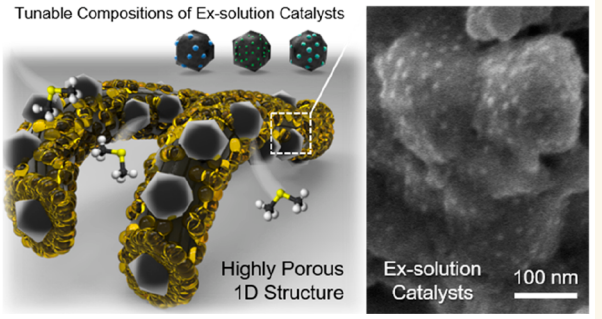

KEYWORDS: *ex-solution, metal alloy, heterogeneous catalysts, hybrid catalysts, gas sensors*

The surface-embellishment of materials with catalytic nanoparticles (NPs), forming supported catalysts,[1] has been considered as a pivot role in various industrial fields such as petroleum refining, three-way catalysis,[2] fuel cell/electrolyzers,[3] photocatalysts, and gas sensors.[4] In such system, smaller NPs must be spread evenly throughout the support crystals to maximize catalyst dispersion and utilization, while minimizing their agglomeration during synthesis and operation.[5] However, the conventional methods such as deposition techniques (e.g., chemical impregnation, vacuum-based vapor deposition) for fabricating supported catalysts make it difficult to achieve the aforementioned requirements.

In this regard, the surface self-precipitation of metal NPs from the lattice of reservoir scaffold oxides, the "ex-solution" phenomenon, fascinated many engineers as a platform for fabricating supported catalysts, allowing uniform particle distribution and enhanced chemical/thermal durability.[6] Despite the many engaging advantages of the ex-solution process, high-temperature heat treatment (>700 °C) in reductive gas atmosphere to extrude doped metal cations limits the diversity of structural and compositional choices in applicable materials.[6,7] In particular, such high heat treatment prevents the host oxide from maintaining a porous nanoscale structure and often causes decomposition of the oxide.

Such disadvantages are particularly noticeable in applications such as surface-reaction dominated metal oxide-based gas sensors where target analytes should be facilely diffused into the oxide structure to dynamically react with adsorbed oxygen species even at low concentrations (e.g., ppb or ppm level).[8] For example, Wang's group reported NO_2 and NH_3 gas sensing layers using $LaFePd_{0.05}O_{3+\delta}$ and $AgNbO_3$ perovskite oxides functionalized with ex-solved PdO and Ag particles,

Received: December 19, 2022
Accepted: March 10, 2023
Published: March 14, 2023

https://doi.org/10.1021/acsnano.2c12580
ACS Nano 2023, 17, 5842−5851

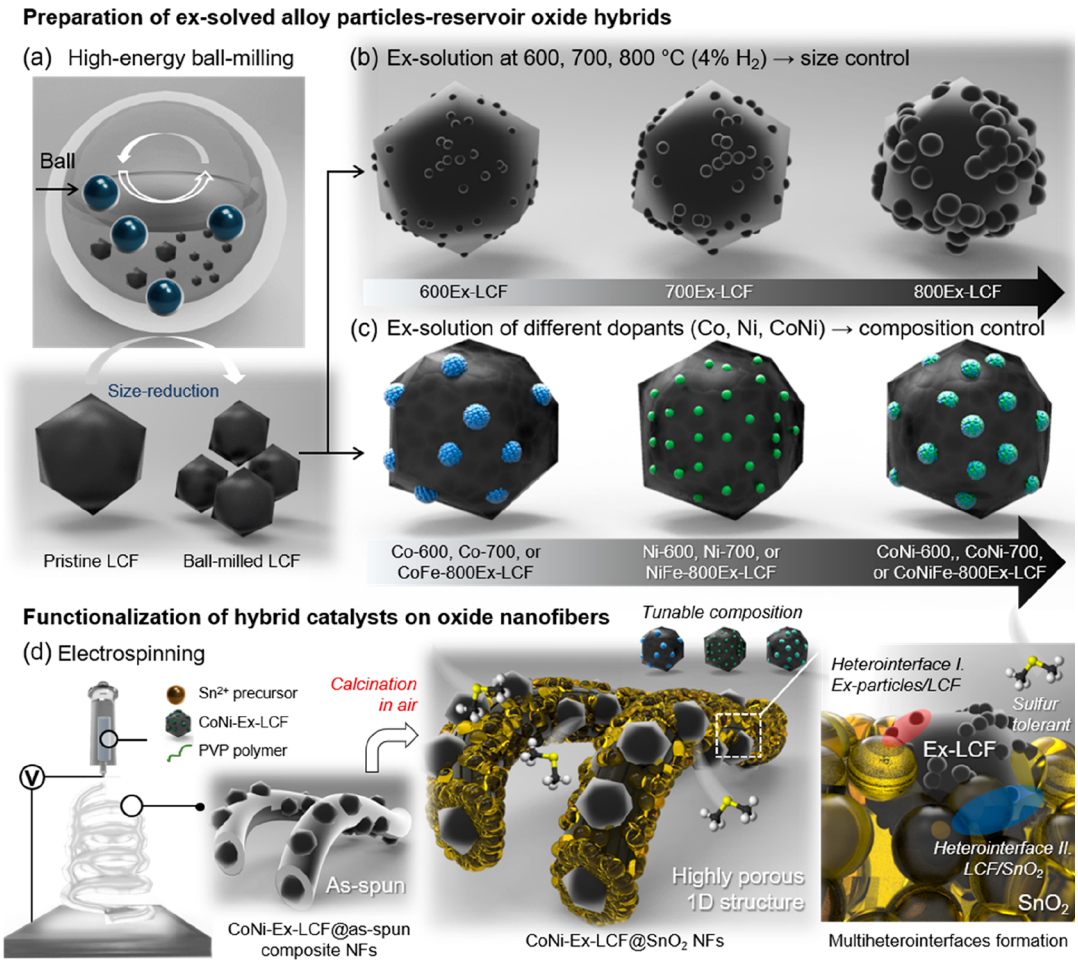

Figure 1. Schematic illustrations of the preparation of ex-solved alloy particles-reservoir oxide hybrids (i.e., ex-solution hybrids) and functionalization on oxide nanofibers via an electrospinning process. (a) High-energy ball-milling process for size-reduction of doped LCF perovskite particles. (b) Control of the size distribution of ex-solved particles depends on the ex-solution temperatures. (c) Control of the composition of ex-solved particles by varying the dopant compositions. (d) Electrospinning process to functionalize ex-solution hybrids on porous one-dimensional oxide nanofiber scaffolds.

respectively.[9] Both host materials are stable in reductive conditions but unable to give the significant sensitivity and detection limit due to low electrical conductivity and insufficient surface area of typical perovskite-type ex-solution materials. Unfortunately, most common state-of-the-art sensing materials such as SnO_2, ZnO, and Fe_2O_3 are not suitable for ex-solution reservoir oxides because of phase instability in reductive conditions, which is the inevitable material property for ex-solution processes.

To address the aforementioned obstacles of the conventional ex-solution process, here, we devise the design principle in which the "ex-solution hybrids", i.e., ex-solved NPs-decorated reservoir oxides, are functionalized at the surface of a porous nanoscale framework. Such method can be described by following two steps: (1) synthesis of ex-solution hybrids by reductive heat treatment of reservoir oxides and (2) functionalization of host oxide scaffolds with the as-prepared ex-solution catalysts. For this purpose, we selected the $LaFeO_3$-based perovskite (i.e., $La_{0.6}Ca_{0.4}FeO_{3-\delta}$, LCF) particles as a reservoir and the SnO_2 nanofibers (NFs), which would decompose easily at low temperature in reductive atmosphere, as a porous host scaffold.[10,11] Then, by adjusting doping types (e.g., Co, Ni, and CoNi, total 5 at%) in reservoir oxide and ex-solution conditions, we investigated the gas sensing characteristics toward seven different gas analytes including dimethyl sulfide (DMS, C_2H_6S), methyl mercaptan (CH_3SH), hydrogen sulfide (H_2S), acetone (C_3H_6O), carbon monoxide (CO), ammonia (NH_3), and methane (CH_4). Our observation suggested that alloy metal NPs (e.g., CoFe, NiFe, and CoNiFe) were successfully extruded on the LCF reservoir when annealed at 800 °C (in 4% H_2/Ar) and that the SnO_2 NFs were homogeneously functionalized with ex-solution catalysts via an electrospinning method. In addition, the resulting materials, i.e., SnO_2 NFs decorated by ex-solution hybrids which contain CoNiFe NPs, showed exceptional gas sensing properties (148 @ 5 ppm) with excellent cycling stability (116 cycles) and long-term (8-months) stability in DMS gas detection. Moreover, we simply changed the ex-solution hybrid materials to Co-ex-solved $La_{0.6}Sr_{0.4}Mn_{0.85}Co_{0.15}O_{3-\delta}$, and we found that they led to highly selective CH_3SH gas sensing characteristics, demonstrating facile tunability of catalytic reactions. Altogether, this alternative approach enables robust synthesis and a broad range of materials combination of "porous host oxide scaffold sensitized by ex-solved alloy metal NPs-reservoir oxide", leading to expanding of the potential ranges of ex-solution-based catalysts and superior gas sensing performance.

https://doi.org/10.1021/acsnano.2c12580
ACS Nano 2023, 17, 5842−5851

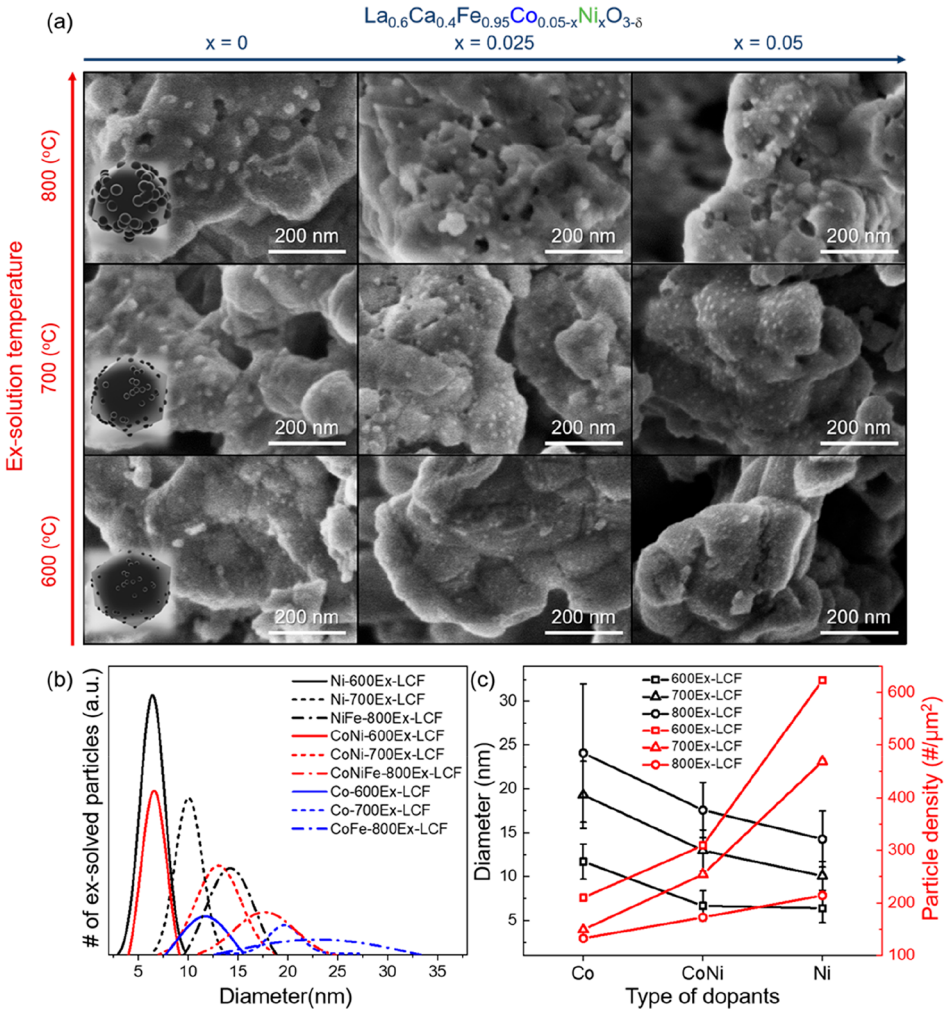

Figure 2. (a) SEM images of controlled sizes and densities of Co, Ni, or CoNi particles ex-solved on $La_{0.6}Ca_{0.4}Fe_{0.95}O_{3-\delta}$ (LCF) particles at various temperatures and dopant compositions. (b–c) Quantitative analyses of ex-solved Co, Ni, or CoNi particles. Diameter and particle density of ex-solved particles depends on ex-solution temperature and type of dopants.

RESULTS AND DISCUSSION

Preparation of Oxide Nanofibers Functionalized with Ex-Solution Hybrids. The schematics in Figure 1 illustrate the synthetic procedures of the various ex-solved alloy particles-reservoir oxide catalysts (i.e., ex-solution hybrids) and their functionalization on oxide NFs via an electrospinning technique. First, we synthesized 5 at% of Co-doped, Ni-doped and CoNi-doped LCF by the conventional sol–gel process. Then, we conducted the high-energy ball-milling process of doped LCF perovskites to reduce the particle size (Figure 1a, see details in Experimental Section). Bare LCF perovskites exhibit about 200–500 nm of relatively large size distributions (Figure S1). Meanwhile, after the ball-milling process, the size of LCF perovskites decreased (100–200 nm) and correspondingly, the BET surface area increased from 1.82 to 5.77 $m^2\ g^{-1}$ (Figure S2). Subsequently, the ex-solution process is followed with the aid of systematic engineering of the ex-solution temperatures (600, 700, and 800 °C) and types of dopants (Co, Ni and CoNi) to control the size and composition of ex-solved particles (Figure 1b–c). Interestingly, note that Fe element is also extruded from the LCF perovskite support to form CoFe, NiFe, and CoNiFe alloy ex-solved NPs systems after annealing at 800 °C (The details will be explained in Figure 3). Finally, we functionalize the as-prepared hybrid catalysts on oxide NFs by using the single-spinneret electrospinning technique (Figure 1d). The electrospinning solution is prepared by mixing Sn-precursor, polyvinylpyrrolidone (PVP) polymer, and ex-solution hybrids in dimethylformamide (DMF) solvent; then electrospinning is conducted to prepare as-spun ex-solution catalysts/Sn-precursor/PVP polymer composite NFs. After calcination at 500 °C for 1 h in air atmosphere, the ex-solution hybrid catalyst-functionalized SnO_2 NFs were obtained, where ex-solved NPs/LCF reservoir oxide and LCF/SnO_2 build-up multi-heterointerfaces to modulate the intrinsic electrochemical properties.

Physical and Chemical Characterizations of Ex-Solution Hybrids. To investigate the metal particle formation behavior of the ball-milled LCF oxide reservoirs according to dopant types and ex-solution temperatures, three series of doped-LCF perovskite oxides are heat-treated in dry 4% H_2/Ar gases at temperatures ranging from 600 to 800 °C for 2 h. The samples are named according to the aforementioned control variables (e.g., Co-600Ex-LCF denotes the Co-doped LCF ex-solution at 600 °C, and CoFe-800Ex-LCF denotes the Co-doped LCF ex-solution at 800 °C). Figure 2a shows the pseudo-surface-phase diagram describing how the surface of reservoir oxides varies by the ex-solution process after a reduction at given conditions (e.g., different dopants and

https://doi.org/10.1021/acsnano.2c12580
ACS Nano 2023, 17, 5842–5851

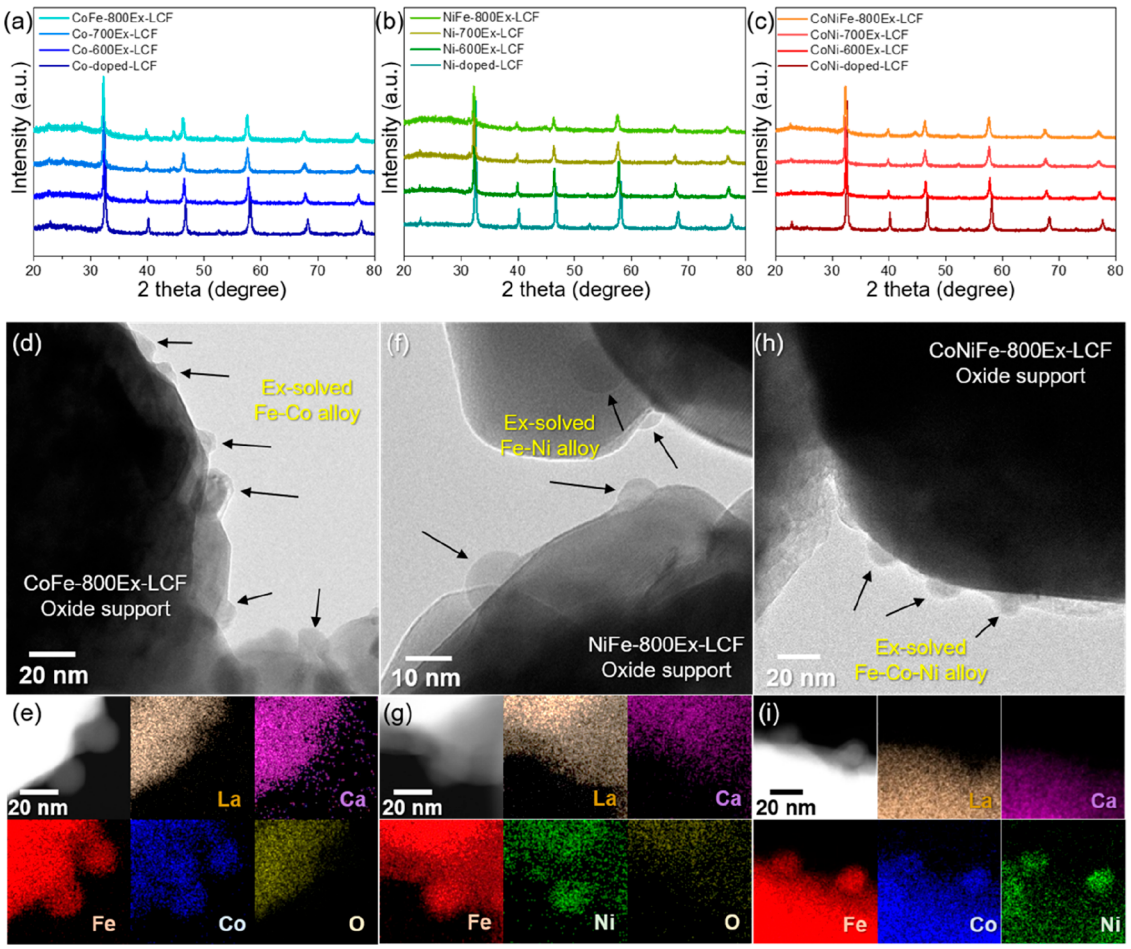

Figure 3. XRD analysis of (a) Co-, (b) Ni-, and (c) CoNi-Ex-LCF particles at various ex-solution temperatures (pristine and 600, 700, and 800 °C). TEM, STEM, and EDS mapping images of (d−e) CoFe-800-Ex-LCF, (f−g) NiFe-800Ex-LCF, and (h−i) CoNiFe-800Ex-LCF particles.

temperatures) through scanning electron microscopy (SEM) observations. It is clearly indicated that catalytically active NPs with a range of diameters (5−35 nm) were successfully produced on each oxide on every experimental condition. By employing SEM images as shown in Figure 2a, the size distributions of observed ex-solution NPs were quantitatively analyzed (Figure 2b−c). The detailed size distributions of ex-solution particles, along with analyzed images and methods are described in Figures S3−S5. As the temperature of the ex-solution reaction increases, the size of extruded particles also increases while the number density decreases regardless of the dopant types (Figure 2b). Such tendency can be found in various references on powder-type samples. On the other hand, it is noteworthy that the particle size distributions are significantly influenced by the dopant types. For example, under the same annealing condition, ex-solved Co-doped LCF series exhibit the largest particle size and the smallest number density; in contrast, ex-solved Ni-doped LCF series show the opposite trend in terms of particle size and number density (Figure 2c). In addition to this, the size and number density of ex-solution particles from the CoNi-doped LCF starting material were positioned between the aforementioned two samples.

The crystal structures of all the series of pristine and ex-solved LCF reservoirs were confirmed by the high-resolution powder X-ray diffraction (HRXRD) measurement (Figure 3a−c). The diffraction results reveal that the Co-doped, Ni-doped, and CoNi-doped LCF have the orthorhombic perovskite structure, with a tiny shift of the overall diffraction patterns (Figure S6a) due to the different oxidation states and ionic radii of the dopants compared to those of the Fe host in LCF. Such perovskite structures were preserved even after harsh reductive heat treatments, accompanying the lowering of the Bragg's angle position (i.e., increase of lattice volume) as shown in Figure S6b−d. More lattice expansion was found as the reduction temperatures increased, and such a phenomenon may be attributed to the formation of oxygen vacancies. Furthermore, the peak assigned as a metallic phase (i.e., $2\theta \sim 44.7°$) after the ex-solution process was only detected after 800 °C annealing even though the particle ex-solution has occurred at both 600 °C- and 700 °C-annealed samples. This result indicates that as the annealing temperature increases, more metallic particles are precipitated on the oxide surface, which is consistent with other literature.[12]

To clearly observe the surface microstructure of the LCF reservoirs and the composition of the ex-solved NPs, we conducted transmission electron microscopy (TEM) analysis. Figures 3d, 3f and 3h are the TEM images of CoFe-800Ex-LCF, NiFe-800Ex-LCF and CoNiFe-800Ex-LCF, respectively. As shown in these images, it is clearly shown that the spontaneously formed particles are strongly socketed at each of the LCF support oxides, which is a characteristic feature of ex-

https://doi.org/10.1021/acsnano.2c12580
ACS Nano 2023, 17, 5842−5851

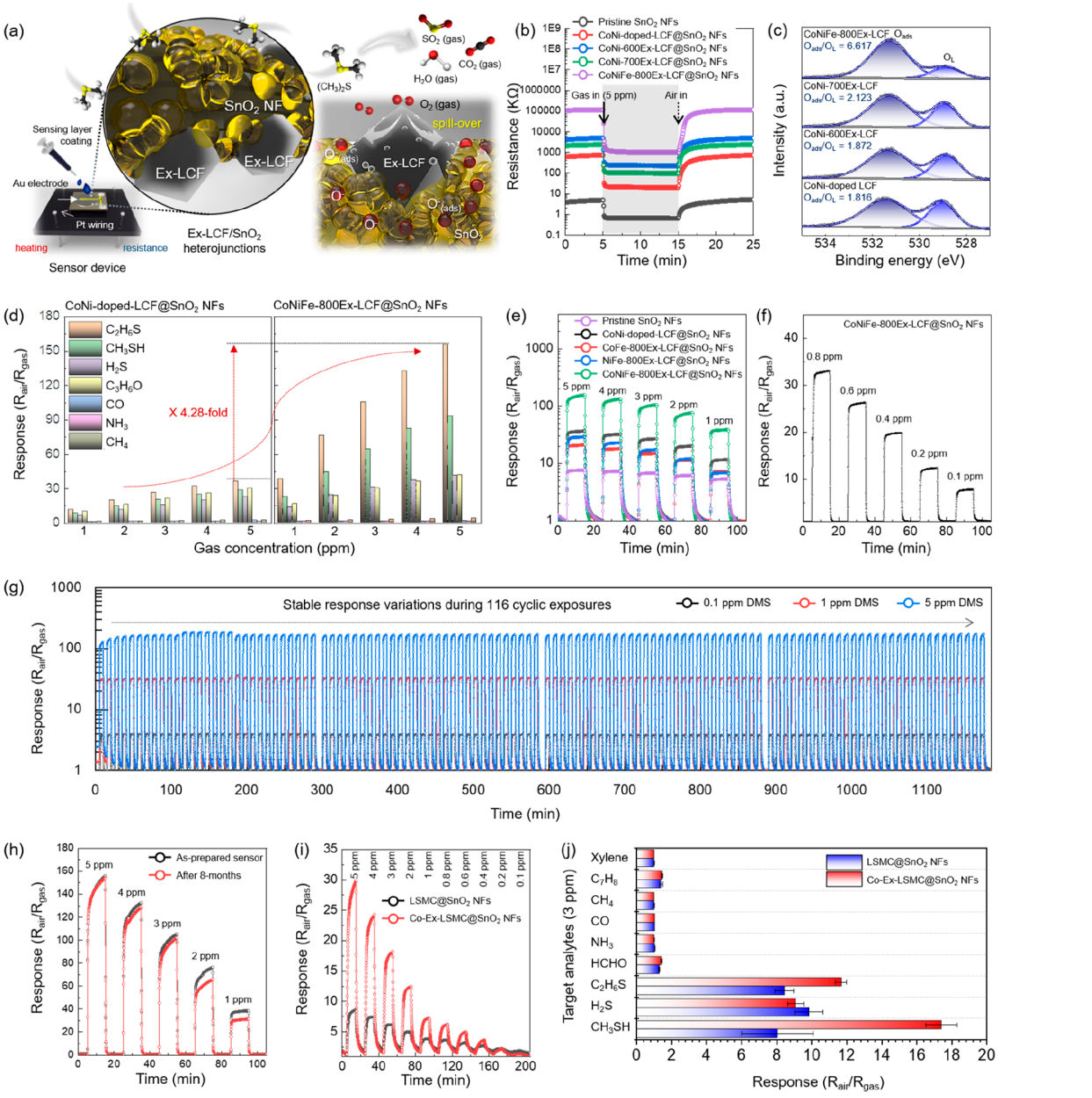

Figure 4. (a) Schematic illustrations of the sensor device coated with sensing layers. (b) Dynamic resistance transition of pristine SnO_2 NFs, CoNi-doped-LCF@SnO_2 NFs, CoNi-600Ex-LCF@SnO_2 NFs, CoNi-700Ex-LCF@SnO_2 NFs, and CoNiFe-800Ex-LCF@SnO_2 NFs. (c) XPS analysis of CoNi-doped LCF, CoNi-600Ex-LCF, CoNi-700Ex-LCF, and CoNiFe-800Ex-LCF at O 1*s* spectra. (d) Selective detection characteristics of CoNi-doped-LCF@SnO_2 NFs and CoNiFe-800Ex-LCF@SnO_2 NFs toward 7 different gas analytes. (e) Dynamic dimethyl sulfide (DMS) sensing response characteristics in the concentration range of 5−1 ppm. (f) Dynamic DMS sensing response characteristics of CoNiFe-800Ex-LCF@SnO_2 NFs in the concentration range of 0.8−0.1 ppm. (g) Long-cycling stability of CoNiFe-800Ex-LCF@SnO_2 NFs toward 0.1, 1, and 5 ppm DMS for 116 cycles at 350 °C. (h) Long-term stability tests of CoNi-800Ex-LCF@SnO_2 NFs using as-prepared and after 8-month sensors. (i) Dynamic CH_3SH sensing characteristics in the concentration range of 5−0.1 ppm using LSMC@SnO_2 NFs and Co-Ex-LSMC@SnO_2 NFs. (j) Selective detection characteristics toward 9 different interfering gas analytes.

solution catalysts. Then, we examined the composition of ex-solved NPs by energy dispersive X-ray spectroscopy (EDS) measurement (Figures 3e, 3g, and 3i). The EDS mapping results indicate that all of the particles are in the form of metal alloys, e.g., binary CoFe, NiFe and ternary CoNiFe alloy particles. Moreover, based on the EDS spectrum, we evaluated the detailed composition of the particle. To ensure reliability of the particle composition obtained from TEM-EDS data and to account for any interference from the host oxide as well as particle heterogeneity, we conducted measurements of multiple ex-solution particles located at the sample's edge and calculated their average value (Figures S7−S9). The resulting average compositions are Fe(77.7 ± 5.6 at%):Co(22.3 ± 5.6 at %), Fe(75.2 ± 7.8 at%):Ni(24.8 ± 7.8 at%), and Fe(75.6 ± 4.4 at%):Co(5.0 ± 1.7 at%):Ni(19.4 ± 4.5 at%), respectively (Tables S1−S3). Note that in the case of CoNi-600Ex-LCF and CoNi-700Ex-LCF, the ex-solved alloy particles tend to form without Fe species, indicating that the ex-solution temperature should be as high as 800 °C to form ternary CoNiFe alloy particles (Figure S10).

https://doi.org/10.1021/acsnano.2c12580
ACS Nano 2023, 17, 5842−5851

Preparation of Ex-Solution Hybrids@SnO_2 NFs and Gas Sensing Case Study. After electrospinning of ex-solution hybrids (5 wt%)-loaded electrospinning solution, followed by a calcination process in air atmosphere (500 °C for 1 h), ex-solution hybrids-decorated SnO_2 nanofibers (hereafter ex-solution hybrids@SnO_2 NFs) were obtained (e.g., CoNiFe-800Ex-LCF@SnO_2, Figure S11). The as-spun composite NFs exhibit mostly smooth, but partially bumpy, surface morphologies derived from the embedded CoNiFe-800Ex-LCF particles (Figure S11a). After calcination in air atmosphere, the Sn precursor is oxidized to form nanogranular SnO_2, where CoNiFe-800Ex-LCF particles are well-embedded in SnO_2 NFs to construct heterointerfaces, i.e., ex-solution catalysts-LCF and ex-solution hybrids-SnO_2 (Figures S11b–c). The pristine SnO_2 NFs showed smooth surface morphologies and densely packed nanofiber structures with SnO_2 nanograins (Figure S12). To understand the thermal decomposition behaviors of as-spun composite NFs during the calcination process in air atmosphere, we further conducted the thermal gravimetric (TG) and differential scanning calorimetric (DSC) analyses using as-spun Sn precursor/PVP composite NFs and as-spun CoNiFe-800Ex-LCF/Sn precursor/PVP composite NFs (Figure S13). The results showed that thermal decomposition of PVP polymer and oxidation of Sn precursor to SnO_2 occur at about 300 and 500 °C, respectively, proving that 500 °C of calcination temperature is appropriate to form crystalline SnO_2, as demonstrated in XRD analysis (Figure S14).

The sensing materials, e.g., CoNi-Ex-LCF@SnO_2 NFs, were drop-coated on the Al_2O_3 substrate which is patterned with parallel Au electrodes (25 μm and 70 μm of width and separation distance, respectively), and the sensing characteristics were analyzed using the homemade sensor measurement system (Figure 4a and Figure S15). We hypothesized that construction of NPs with diverse elements would introduce unexpectedly high catalytic performances that are not found in their single-phase catalyst counterparts. In this regard, we focused on the evaluation of the sensing performances using SnO_2 NFs functionalized with CoNi-Ex-LCF-based heterogeneous catalysts, i.e., CoNi-600Ex-LCF, CoNi-700Ex-LCF, and CoNiFe-800Ex-LCF. First, to investigate the role of ex-solved CoNi-doped LCF series catalysts with controlled ex-solution temperatures, we conducted dynamic resistance transitions upon exposure to 5 ppm dimethyl sulfide (DMS) gas using five different sensors: pristine SnO_2 NFs, CoNi-doped-LCF@SnO_2 NFs, CoNi-600Ex-LCF@SnO_2 NFs, CoNi-700Ex-LCF@SnO_2 NFs, and CoNiFe-800Ex-LCF@SnO_2 NFs (Figure 4b). The sensing tests were conducted in highly humid conditions (90% RH), since the precise detection of a trace amount of DMS gas is important for the diagnosis of extra-oral disease from the exhaled breath of patients (Figure S16).[13] Note that H_2S and CH_3SH are related with intraoral halitosis while DMS is closely related with extra-oral halitosis; thus, it is important to discriminately detect three different sulfuric compounds. The sensing mechanisms of n-type metal oxides-based sensing layers heavily depend on the modulation of the amount of chemisorbed oxygen species (O^-_{ads}) on the surface of oxides which either build-up the electron depletion region in air atmosphere or donate back the electrons to the conduction band of oxides in reactions with reducing gases.[14] Recently, it was reported that some perovskite particles dissociate oxygen molecules and diffuse them into the neighboring oxide supports.[10,15] Similar to these reports, CoNi-doped-LCF@SnO_2 NFs showed drastically increased baseline resistance (737.8 kΩ) than that (4.9 kΩ) of the pristine SnO_2 NFs, meaning that a high density of oxygen molecules are chemisorbed on the SnO_2 NFs through CoNi-doped-LCF catalysts. Furthermore, ex-solved metallic NPs can also act as spillover catalysts; thus, CoNi-600Ex-LCF@SnO_2 NFs and CoNi-800Ex-LCF@SnO_2 NFs showed 6.7-fold and 156.2-fold increased baseline resistance than CoNi-doped-LCF@SnO_2 NFs.[16] To understand the spillover effect of ex-solution catalysts, we conducted the X-ray photoelectron spectroscopy (XPS) analysis at O 1*s* spectra with four different LCF particles including CoNi-doped-LCF, CoNi-600Ex-LCF, CoNi-700Ex-LCF, and CoNi-800Ex-LCF (Figure 4c). The results showed that the ratio between adsorbed oxygen species (O_{ads}, O^-) and lattice oxygen (O_L, O^{2-}), i.e., (O_{ads}/O_L), dramatically increased to 6.617 in the case of CoNi-800Ex-LCF compared with those (1.816, 1.872, and 2.123) of CoNi-doped-LCF, CoNi-600Ex-LCF, and CoNi-700Ex-LCF, respectively, which were calculated from the peak area values of XPS analysis at O 1*s* spectra (Figure 4c and Table S4). The higher O_{ads}/O_L value of CoNi-800Ex-LCF is well-matched with the increased baseline resistance of CoNi-800Ex-LCF@SnO_2 NFs sensors.

The gas sensing selectivity is an important factor that high-performance chemiresistive gas sensors should possess.[17] In this sense, the selective detection characteristics were analyzed at 350 °C toward seven different gas analytes including dimethyl sulfide (DMS, C_2H_6S), methyl mercaptan (CH_3SH), hydrogen sulfide (H_2S), acetone (C_3H_6O), carbon monoxide (CO), ammonia (NH_3), and methane (CH_4) using CoNi-doped-LCF@SnO_2 NFs and CoNi-800Ex-LCF@SnO_2 NFs (Figure 4d). Before the ex-solution process, the CoNi-doped-LCF@SnO_2 NFs sensor exhibited poor selectivity showing similar responses (36.4, 28.5, 22.8, and 30.0) toward 5 ppm of DMS, CH_3SH, H_2S, and acetone, respectively. Meanwhile, the CoNi-800Ex-LCF@SnO_2 NFs sensor showed not only improved selectivity toward DMS gas but also enhanced response (4.28-fold improvement @ 5 ppm) than that of CoNi-doped-LCF@SnO_2 NFs. It is shown that the ex-solution temperature is important to endow with DMS selectivity, since the CoNi-600Ex-LCF@SnO_2 NFs and CoNi-700Ex-LCF@SnO_2 NFs sensors showed poor DMS selectivity and sensitivity (Figure S17). It is expected that the formation of ex-solved CoNiFe alloy NPs can accelerate spillover of O_2 and DMS gas toward the neighboring SnO_2 matrix to effectively modulate its electrical conductivity.[15] Since the CoNi-800Ex-LCF@SnO_2 NFs sensor showed selective sensing characteristics toward sulfur-containing molecules, e.g., DMS, we further analyzed the temperature-dependent sensing properties toward three different sulfuric compounds (DMS, CH_3SH, and H_2S) at 300, 325, 350, and 375 °C (Figure S18a). At each temperature, the selectivity factor (R_{DMS}/R_{CH3SH} or R_{DMS}/R_{H2S}, where R_{DMS}, R_{CH3SH}, and R_{H2S} denote the response toward DMS, CH_3SH, and H_2S, respectively) was calculated (Figure S18b). After determining the optimal temperature to be 350 °C based on the response and selectivity factor, we further investigated the DMS sensing properties of various ex-solved NPs, including pristine SnO_2 NFs, CoNi-doped-LCF@SnO_2 NFs, Ni-700Ex-LCF@SnO_2 NFs, Co-700Ex-LCF@SnO_2 NFs, CoNi-700Ex-LCF@SnO_2 NFs, CoFe-800Ex-LCF@SnO_2 NFs, NiFe-800Ex-LCF@SnO_2 NFs, and CoNiFe-800Ex-LCF@SnO_2 NFs upon exposure to 5–1 ppm gas (Figure 4e and Figure S19). As a result, CoNi-doped-LCF@SnO_2 NFs showed 4.8- and 2.2-fold improved response than pristine SnO_2 NFs at 5 and 1 ppm DMS, respectively. Based on the synergistic effects of ex-solved

https://doi.org/10.1021/acsnano.2c12580
ACS Nano 2023, 17, 5842–5851

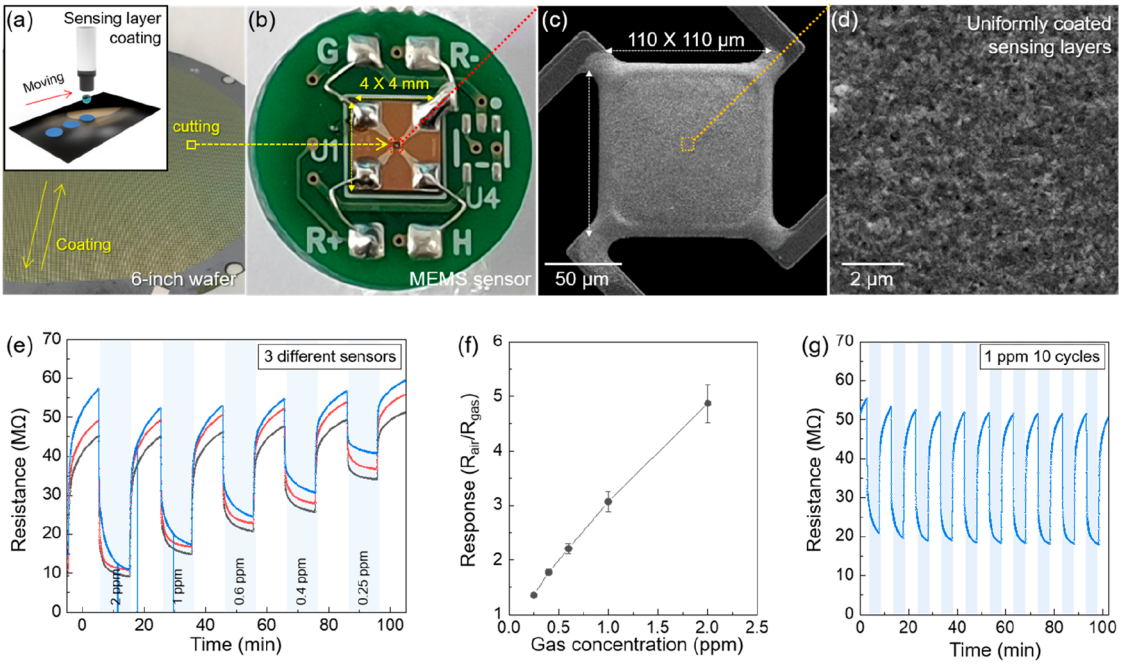

Figure 5. (a) Schematic illustrations, (b) photography images, and (c–d) SEM images of the MEMS sensor coated with CoNiFe-800Ex-LCF@SnO_2 NFs-based sensing layers using the EHD coating method on a Si wafer (6 in.). (e–f) Dynamic sensing characteristics of three different MEMS sensors toward 2–0.25 ppm DMS and (g) cyclic exposure to 1 ppm DMS for 10 cycles.

CoNiFe alloy NPs and oxygen deficient LCF perovskites, CoNiFe-800Ex-LCF@SnO_2 NFs showed superior response (148.3 and 38.5 at 5 and 1 ppm, respectively), which is even 4.1- and 3.3-fold higher than that of CoNi-doped-LCF@SnO_2 NFs. In terms of low-concentration (0.8–0.1 ppm) DMS sensing capabilities, CoNiFe-800Ex-LCF@SnO_2 NFs sensors showed reasonably high response, e.g., R_{air}/R_{gas} = 7.8 @ 100 ppb (Figure 4f). Moreover, CoNiFe-800Ex-LCF@SnO_2 NFs displayed a response time of 6 s toward 5 ppm DMS gas, indicating that the opened porous structures of oxide NFs and high catalytic activities of CoNiFe ex-solved alloy particles enable fast diffusion and dissociation of target gas analytes (Figure S20).[18]

One of the strong advantages of the ex-solution catalysts is their superior chemical/thermal durability even under harsh operating conditions such as high temperature or oxidative sulfuric atmosphere.[19] Conventional metal oxide-based chemiresistive gas sensors usually suffer from poor stability under high operating temperature with long-cycling conditions, since the catalysts are easily agglomerated and in turn lead to deterioration in catalytic activity. In this regard, CoNiFe-800Ex-LCF@SnO_2 NFs sensors pose strong advantages in stability based on effective socketing of ex-solved CoNiFe alloy particles on LCF supports which are anchored on the SnO_2 NFs matrix. During long-cycling stability tests (116 cycles) toward 0.1, 1, and 5 ppm DMS gas, respectively, the sensors maintained their exceptional stability in DMS sensing responses (Figure 4g). Furthermore, even after 8-months of aging period, CoNiFe-800Ex-LCF@SnO_2 sensors maintained the response without severe degradation in sensing characteristics, proving the excellent long-term stability (Figure 4h). Compared with the state-of-the-art works of previously reported metal oxide-based chemiresistive DMS gas sensors, CoNiFe-800Ex-LCF@SnO_2 NFs showed superior sensing performances in terms of response, response time, detection limit, and long-term cyclability/stability (Table S5).

We further demonstrated that, in addition to CoNi-Ex-LCF, other types of ex-solved alloy particles-reservoir oxide hybrids could also be utilized as effective catalysts to improve the sensing characteristics of metal oxides. As a case study, we modified the standard protocol slightly to prepare LSMC@SnO_2 NFs and Co-Ex-LSMC@SnO_2 NFs, where LSMC denotes $La_{0.6}Sr_{0.4}Mn_{0.85}Co_{0.15}O_{3-\delta}$, and evaluated their sensing properties. Note that in Co-Ex-LSMC hybrid catalysts, ex-solved Co NPs in LSMC reservoir oxides exhibit ultrasmall (<5 nm) and uniform distributions as shown in the SEM images (Figure S21). Moreover, the crystal structure of LSMC was preserved after the ex-solution process as shown in Figure S22. As a result, Co-Ex-LSMC@SnO_2 NFs showed about 7.5-fold increased baseline resistance (1.5 MΩ) than that of pristine LSMC@SnO_2 NFs based on effective catalytic sensitization effects, i.e., spillover (Figure S23). Moreover, Co-Ex-LSMC@SnO_2 NFs exhibited dramatically enhanced response characteristics toward CH_3SH gas analytes, showing a response of 29.9 toward 5 ppm of CH_3SH, which is 3.5-fold higher than that of pristine LSMC@SnO_2 NFs (Figure 4i and Table S6). In particular, pristine LSMC@SnO_2 NFs feature poor selective gas sensing properties, showing similar responses toward three different sulfur containing molecules, including H_2S, CH_3SH, and C_2H_6S, while Co-Ex-LSMC@SnO_2 NFs showed excellent selectivity toward CH_3SH analytes (Figure 4j). There is potential feasibility to discriminate DMS (biomarker of extraoral halitosis) and CH_3SH (biomarker of intraoral halitosis) analytes by combining the CoNiFe-Ex-LCF@SnO_2 NFs- and Co-Ex-LSMC@SnO_2 NFs-based sensing layers as an array-type sensor platform. We believe that our synthetic strategies of loading ex-solved particles-reservoir oxide hybrids on nanostructured oxide supports could be extended to other systems by simply utilizing different combinations of catalyst and support materials for the development of high-performance sensing layers for the detection of gas analytes with tunable selectivity.

https://doi.org/10.1021/acsnano.2c12580
ACS Nano 2023, 17, 5842–5851

Development of Micro-electromechanical System (MEMS)-Based Sensors. Based on the successful demonstration of ex-solved alloy particles-reservoir oxide hybrids on SnO_2 NFs as effective sensing materials, we further integrated the sensing layers with a microelectromechanical system (MEMS) to fabricate a commercially viable sensor device. After the gram-scale mass-production of the sensing materials, taking advantage of the facile electrospinning synthetic method, the inks including CoNiFe-800Ex-LCF@SnO_2 NFs were coated on a Si wafer (6-in. scale), consisting of about eight thousand MEMS electrodes (110 × 110 μm), via an electrohydrodynamic (EHD)-based dispensing coating route (Figure 5a–d). Note that the MEMS-based sensor device features about 10 mW of low-power consumption, which is about 35-fold lower power than that (~350 mW) of the conventional alumina substrate-based sensor device. We successfully demonstrated the potential feasibility of the MEMS sensors to detect DMS gas in good sensing capabilities during low-concentration (2–0.25 ppm) exposure tests and cyclic (10 cycles) exposure tests (Figure 5e–g). Despite the fact that further optimization progress will be required in the fabrication of MEMS sensor devices, we successfully demonstrated progress in the potential commercialization of our sensing materials using an advanced MEMS-based sensor platform to detect toxic gas analytes.

CONCLUSIONS

We systematically studied the fabrication of ex-solved alloy NPs on reservoir oxides, exemplified by ex-solved CoNiFe on LCF perovskites, via precise control of the ex-solution temperatures and types of dopants. Then, such prepared ex-solution hybrids were successfully functionalized on highly porous SnO_2 NFs using an electrospinning approach. The resulting materials, CoNiFe-800Ex-LCF@SnO_2 NFs, featured exceptional DMS gas sensing properties (R_{air}/R_{gas} ~ 148 @ 5 ppm) with excellent selectivity and long-term/cycle stability based on high catalytic activities of ex-solved CoNiFe alloy NPs, which were demonstrated by comprehensive sensing experiments. Our materials showed potential feasibility toward commercialization based on integration with advanced MEMS devices. We further demonstrated that simple control of the compositions of the ex-solution hybrid (i.e., Co ex-solved LSMC) could effectively tune the gas selectivity toward CH_3SH. Our concept of introducing an ex-solved alloy NPs-perovskite reservoir of hybrid catalysts on electrospun 1D NFs scaffolds holds great advantages in terms of activating full catalytic effects and to allow for facile diffusion and reactions of target analytes based on the highly porous and large surface area of the active layers. Hence, we find our strategy to be beneficial for various potential applications in fields such as catalysis and sensors.

EXPERIMENTAL SECTION

Preparation of Precursor Materials. Tin chloride dihydrate ($SnCl_2·2H_2O$), N,N-dimethylformamide (DMF, 99.8%), and polyvinylpyrrolidone (PVP, M_w = 1,300,000 g mol^{-1}) were used as received from Sigma-Aldrich (St. Louis, USA).

Preparation of Ex-Solved Alloy Particles-Perovskite Hybrid Catalysts. Reservoir perovskite oxide series such as $La_{0.6}Ca_{0.4}Fe_{0.95}Co_{0.05}O_{3-\delta}$ (Co-doped LCF), $La_{0.6}Ca_{0.4}Fe_{0.95}Ni_{0.05}O_{3-\delta}$ (Ni-doped LCF) and $La_{0.6}Ca_{0.4}Fe_{0.95}Ni_{0.025}Co_{0.025}O_{3-\delta}$ (CoNi-doped LCF) were prepared by the typical sol–gel process. Conventional nitrate powders of $La(NO_3)_3·6H_2O$, $Ca(NO_3)_2·4H_2O$, $Ni(NO_3)_2·6H_2O$, $Co(NO_3)_2·6H_2O$ (Alfa Aesar), and $Fe(NO_3)_3·9H_2O$ (Sigma-Aldrich) were used as precursors. Appropriate amounts of precursors were dissolved in deionized (DI) water. Citric acid (Junsei) was also added in the same batch as a chelating agent with a ratio of metal cations:citric acid = 1:1.1. Additionally, the pH (=7) of the solution was controlled by adding NH_4OH (Junsei). Then, the solution was mixed with a stirring bar for 30 min at room temperature; after that, it was aged at 230 °C for gelation. The obtained gel was fired at 450 °C for 3 h; subsequently, it was calcined at 900 °C for 5 h to obtain the perovskite phase. Then, high-energy ball-milling was conducted using LCF-perovskites with controlled ball-milling conditions: 15 or 30 cycles, in which 40 and 20 min of ball-milling and rest time were introduced, respectively, at each cycle. In detail, 1.5 g of perovskite particles was dispersed in 10 mL of ethanol solvent with mixtures of ZrO_2 balls (d = 6 mm and 3 mm). Finally, to obtain the ex-solution hybrids, reservoir oxides were annealed in the temperature range of 600–800 °C with 100 °C intervals with flowing the 4% H_2/Ar gas for 2 h.

Synthesis of SnO_2 Nanofibers Functionalized with Ex-Solved Alloy Particles-Perovskite Complex Catalyst. To prepare the electrospinning solution, 0.25 g of $SnCl_2·2H_2O$, 0.35 g of PVP, and 8.5 mg of ex-solved alloy particles-perovskite complex catalysts (CoNi-800Ex-LCF) were dispersed in 2.1 mL of DMF solvent. Note that 5 wt% of ex-solution hybrids was added as catalysts with respect to the weight of SnO_2 matrix. Then, electrospinning was carried out using the prepared solution at a direct current (DC) voltage of 10 kV, feeding rate of 0.2 mL min^{-1}, and the constant distance of 15 cm between the syringe nozzle and the stainless-steel collector. After collection of the as-spun composite NFs webs, calcination was conducted at 500 °C for 1 h at a ramping rate of 5 °C min^{-1} under ambient air atmosphere. The resultant material was denoted CoNiFe-800Ex-LCF@SnO_2 NFs.

Physical and Chemical Characterization. Surface morphology characterization was conducted by field-emission scanning electron microscopy (SEM, S4800, Hitachi). X-ray photoelectron spectroscopy (XPS, Sigma Probe, Thermo VG Scientific) with Al Kα radiation (1486.6 eV) was conducted to analyze the chemical bonding states. The crystal structures were characterized by high-resolution powder X-ray diffraction (HRXRD, SmartLab, Rigaku) with Cu Kα (wavelength = 1.54 Å) radiation. Surface areas were analyzed using the Brunauer–Emmett–Teller theory (BET, ASAP2020, Micromeritics). Thermal stability was examined by thermal gravimetric analysis (TGA, Labsys Evo, Setaram). The high-resolution microstructure and EDS mapping analyses were conducted by transmission electron microscopy (TEM, JEM-ARM200F, JEOL).

Evaluation of Gas Sensing Characteristics. First, the ink was prepared by mixing 6 mg of sensing material dispersed in 600 μL of EtOH. Then, the ink was coated on the Al_2O_3 substrate patterned with two-parallel Au electrodes (25 and 70 μm of width and separation distance, respectively). The sensing characteristics of the materials were analyzed using the homemade sensor measurement system (Figure S15). The resistance of the sensors was measured every 4 s by using a data acquisition system (34972A, Agilent) with a 16-channel multiplexer (34902A, Agilent). Then, the measured resistance was converted into response (R_{air}/R_{gas}, where R_{air} = resistance in air and R_{gas} = resistance in target gas). The humidity of the sensing environment was controlled by mixing the humidified air. All the sensors were stabilized in baseline air at least for 2 h, before starting the sensing measurements. The sensing tests were conducted by sequentially exposing the target analytes and baseline air for 10 min, respectively. The operating temperature was controlled by applying a DC voltage (DC power supply, E3647A, Agilent) to the microheater of the sensors, positioned on the back side of the Al_2O_3 substrate.

ASSOCIATED CONTENT

Supporting Information

The Supporting Information is available free of charge at https://pubs.acs.org/doi/10.1021/acsnano.2c12580.

https://doi.org/10.1021/acsnano.2c12580
ACS Nano 2023, 17, 5842–5851

SEM images of bare LCF and doped-LCF particles and of doped-LCF particles after the ball-milling process, SEM images and size distribution analyses of ex-solution particles after ex-solution at 600, 700, and 800 °C, SEM images of ex-solution hybrids@SnO_2 NFs before and after calcination, and SEM images of LSMC and Co-Ex-LSMC particles. TEM-EDS mapping images of doped-LCF particles after the ball-milling process, various ex-solution particles after ex-solution at 600, 700, and 800 °C, and ex-solution hybrids@SnO_2 NFs before and after calcination. BET analysis of doped-LCF particles before and after ball-milling process. XRD analysis of LCF particles, LSMC particles, and LCF-loaded SnO_2 NFs before and after ex-solution process. TG/DSC analysis of pristine and ex-solution hybrids loaded as-spun composite NFs. Gas sensing tests: (i) humidity-dependent sensing properties, (ii) temperature-dependent sensing properties, (iii) response time graph, and others. (PDF)

AUTHOR INFORMATION

Corresponding Authors

WooChul Jung − *Department of Materials Science and Engineering, Korea Advanced Institute of Science and Technology (KAIST), Yuseong-gu, Daejeon 34141, Republic of Korea;* orcid.org/0000-0001-5266-3795; Email: wcjung@kaist.ac.kr

Il-Doo Kim − *Department of Materials Science and Engineering, Korea Advanced Institute of Science and Technology (KAIST), Yuseong-gu, Daejeon 34141, Republic of Korea;* orcid.org/0000-0002-9970-2218; Email: idkim@kaist.ac.kr

Authors

Dong-Ha Kim − *Department of Materials Science and Engineering, Korea Advanced Institute of Science and Technology (KAIST), Yuseong-gu, Daejeon 34141, Republic of Korea;* Present Address: (D.-H.K.) Department of Chemistry, Massachusetts Institute of Technology, 77 Massachusetts Avenue, Cambridge, Massachusetts 02139, United States

Jun Kyu Kim − *Department of Materials Science and Engineering, Korea Advanced Institute of Science and Technology (KAIST), Yuseong-gu, Daejeon 34141, Republic of Korea*

DongHwan Oh − *Department of Materials Science and Engineering, Korea Advanced Institute of Science and Technology (KAIST), Yuseong-gu, Daejeon 34141, Republic of Korea*

Seyeon Park − *Department of Materials Science and Engineering, Korea Advanced Institute of Science and Technology (KAIST), Yuseong-gu, Daejeon 34141, Republic of Korea*

Yong Beom Kim − *Department of Materials Science and Engineering, Korea Advanced Institute of Science and Technology (KAIST), Yuseong-gu, Daejeon 34141, Republic of Korea*

Jaehyun Ko − *Department of Materials Science and Engineering, Korea Advanced Institute of Science and Technology (KAIST), Yuseong-gu, Daejeon 34141, Republic of Korea*

Complete contact information is available at: https://pubs.acs.org/10.1021/acsnano.2c12580

Author Contributions

†D.-H.K. and J.K.K. contributed equally

Notes

The authors declare no competing financial interest.

ACKNOWLEDGMENTS

This work was supported by the Technology development Program (S3178295) funded by the Ministry of SMEs and Startups (MSS, Korea). This work was also supported by the Korea Technology and Information Promotion Agency for SMEs (Grant Number: 00141845). This work was supported by the National Research Foundation of Korea (NRF) grant funded by the Korea government (MSIT) (Grant No. 2020R1A2C301312711, and 2022M3H4A1A01008918) and by the Ceramic Strategic Technology R&D program through the Korea Institute of Ceramic Engineering & Technolgy (KICET) (grant NTIS no. 1415181794). The authors also acknowledge support from the Samsung Research Funding & Incubation Center of Samsung Electronics under Project Number SRFC-MA1502-52.

REFERENCES

(1) Kim, J. H.; Kim, J. K.; Liu, J.; Curcio, A.; Jang, J.-S.; Kim, I.-D.; Ciucci, F.; Jung, W. Nanoparticle Ex-solution for Supported Catalysts: Materials Design, Mechanism and Future Perspectives. *ACS Nano* **2021**, *15* (1), 81−110.

(2) Zheng, N.; Stucky, G. D. A general synthetic strategy for oxide-supported metal nanoparticle catalysts. *J. Am. Chem. Soc.* **2006**, *128* (44), 14278−14280.

(3) Hu, X.; Xie, K. Active and stable Ni/$Cr_2O_{3-\delta}$ cathodes for high temperature CO_2 electrolysis. *J. Power Sources* **2019**, *430*, 20−24.

(4) Jang, J. S.; Kim, J. K.; Kim, K.; Jung, W. G.; Lim, C.; Kim, S.; Kim, D. H.; Kim, B. J.; Han, J. W.; Jung, W. Dopant-Driven Positive Reinforcement in Ex-Solution Process: New Strategy to Develop Highly Capable and Durable Catalytic Materials. *Adv. Mater.* **2020**, *32* (46), 2003983. Park, S.; Oh, D.; Ahn, J.; Kim, J. K.; Kim, D. H.; Kim, S.; Park, C.; Jung, W.; Kim, I. D. Promoting ex-solution from metal-organic framework-mediated oxide scaffold for highly active and robust catalysts. *Adv. Mater.* **2022**, *34*, 2201109. Shin, E.; Kim, D.-H.; Cha, J.-H.; Yun, S.; Shin, H.; Ahn, J.; Jang, J.-S.; Baek, J. W.; Park, C.; Ko, J. Ultrafast Ambient-Air Exsolution on Metal Oxide via Momentary Photothermal Effect. *ACS Nano* **2022**, *16* (11), 18133−18142.

(5) Neagu, D.; Oh, T.-S.; Miller, D. N.; Ménard, H.; Bukhari, S. M.; Gamble, S. R.; Gorte, R. J.; Vohs, J. M.; Irvine, J. T. Nano-socketed nickel particles with enhanced coking resistance grown in situ by redox exsolution. *Nat. Commun.* **2015**, *6* (1), 1−8.

(6) Neagu, D.; Tsekouras, G.; Miller, D. N.; Ménard, H.; Irvine, J. T. In situ growth of nanoparticles through control of non-stoichiometry. *Nat. Chem.* **2013**, *5* (11), 916−923.

(7) Kim, K. J.; Han, H.; Defferriere, T.; Yoon, D.; Na, S.; Kim, S. J.; Dayaghi, A. M.; Son, J.; Oh, T.-S.; Jang, H. M. Facet-dependent in situ growth of nanoparticles in epitaxial thin films: the role of interfacial energy. *J. Am. Chem. Soc.* **2019**, *141* (18), 7509−7517.

(8) Kim, S.-J.; Choi, S.-J.; Jang, J.-S.; Kim, N.-H.; Hakim, M.; Tuller, H. L.; Kim, I.-D. Mesoporous WO3 nanofibers with protein-templated nanoscale catalysts for detection of trace biomarkers in exhaled breath. *ACS Nano* **2016**, *10* (6), 5891−5899. Shin, J.; Choi, S. J.; Lee, I.; Youn, D. Y.; Park, C. O.; Lee, J. H.; Tuller, H. L.; Kim, I. D. Thin-wall assembled SnO_2 fibers functionalized by catalytic Pt nanoparticles and their superior exhaled-breath-sensing properties for the diagnosis of diabetes. *Adv. Funct. Mater.* **2013**, *23* (19), 2357−2367.

(9) Li, X.; Dai, L.; He, Z.; Meng, W.; Li, Y.; Wang, L. Enhancing NH_3 sensing performance of mixed potential type sensors by chemical exsolution of Ag nanoparticle on $AgNbO_3$ sensing electrode. *Sens. Actuators B: Chem.* **2019**, *298*, 126854.
(10) Kang, J.-Y.; Jang, J.-S.; Koo, W.-T.; Seo, J.; Choi, Y.; Kim, M.-H.; Kim, D.-H.; Cho, H.-J.; Jung, W.; Kim, I.-D. Perovskite $La_{0.75}Sr_{0.25}Cr_{0.5}Mn_{0.5}O_{3-\delta}$ sensitized SnO_2 fiber-in-tube scaffold: highly selective and sensitive formaldehyde sensing. *J. Mater. Chem. A* **2018**, *6* (22), 10543−10551.
(11) Kim, D.-H.; Jang, J.-S.; Koo, W.-T.; Kim, I. D. Graphene oxide templating: facile synthesis of morphology engineered crumpled SnO_2 nanofibers for superior chemiresistors. *J. Mater. Chem. A* **2018**, *6* (28), 13825−13834.
(12) Kim, J. K.; Jo, Y.-R.; Kim, S.; Koo, B.; Kim, J. H.; Kim, B.-J.; Jung, W. Exceptional Tunability over Size and Density of Spontaneously Formed Nanoparticles via Nucleation Dynamics. *ACS Appl. Mater. Interfaces* **2020**, *12* (21), 24039−24047. Jo, Y.-R.; Koo, B.; Seo, M.-J.; Kim, J. K.; Lee, S.; Kim, K.; Han, J. W.; Jung, W.; Kim, B.-J. Growth kinetics of individual Co particles Ex-solved on $SrTi_{0.75}Co_{0.25}O_{3-\delta}$ polycrystalline perovskite thin films. *J. Am. Chem. Soc.* **2019**, *141* (16), 6690−6697.
(13) Murata, T.; Yamaga, T.; Iida, T.; Miyazaki, H.; Yaegaki, K. Classification and examination of halitosis. *Int. Dent. J.* **2002**, *52* (S5P1), 181−186. Tangerman, A. Halitosis in medicine: a review. *Int. Dent. J.* **2002**, *52* (S5P1), 201−206. Shin, H.; Kim, D.-H.; Jung, W.; Jang, J.-S.; Kim, Y. H.; Lee, Y.; Chang, K.; Lee, J.; Park, J.; Namkoong, K. Surface activity-tuned metal oxide chemiresistor: toward direct and quantitative halitosis diagnosis. *ACS Nano* **2021**, *15* (9), 14207−14217.
(14) Wang, C.; Yin, L.; Zhang, L.; Xiang, D.; Gao, R. Metal oxide gas sensors: sensitivity and influencing factors. *Sensors* **2010**, *10* (3), 2088−2106. Kim, D.-H.; Cha, J.-H.; Shim, G.; Kim, Y. H.; Jang, J.-S.; Shin, H.; Ahn, J.; Choi, S.-Y.; Kim, I.-D. Flash-thermochemical engineering of phase and surface activity on metal oxides. *Chem.* **2022**, *8* (4), 1014−1033. Yamazoe, N. New approaches for improving semiconductor gas sensors. *Sens. Actuators B: Chem.* **1991**, *5* (1−4), 7−19.
(15) Lin, H.-J.; Baltrus, J. P.; Gao, H.; Ding, Y.; Nam, C.-Y.; Ohodnicki, P.; Gao, P.-X. Perovskite nanoparticle-sensitized Ga2O3 nanorod arrays for CO detection at high temperature. *ACS Appl. Mater. Interfaces* **2016**, *8* (14), 8880−8887.
(16) Kohl, D. The role of noble metals in the chemistry of solid-state gas sensors. *Sens. Actuators B: Chem.* **1990**, *1* (1−6), 158−165.
(17) Morrison, S. R. Selectivity in semiconductor gas sensors. *Sens. Actuators* **1987**, *12* (4), 425−440.
(18) Kim, S.-J.; Choi, S.-J.; Jang, J.-S.; Cho, H.-J.; Kim, I.-D. Innovative nanosensor for disease diagnosis. *Acc. Chem. Res.* **2017**, *50* (7), 1587−1596.
(19) Park, S.; Kim, Y.; Noh, Y.; Kim, T.; Han, H.; Yoon, W.; Choi, J.; Yi, S.-H.; Lee, W.-J.; Kim, W. B. A sulfur-tolerant cathode catalyst fabricated with in situ exsolved CoNi alloy nanoparticles anchored on a Ruddlesden-Popper support for CO_2 electrolysis. *J. Mater. Chem. A* **2020**, *8* (1), 138−148. Papaioannou, E. I.; Neagu, D.; Ramli, W. K.; Irvine, J. T.; Metcalfe, I. S. Sulfur-tolerant, exsolved Fe-Ni alloy nanoparticles for CO oxidation. *Top. Catal.* **2019**, *62* (17), 1149−1156.

https://doi.org/10.1021/acsnano.2c12580
ACS Nano 2023, 17, 5842−5851